SOME DYNAMICAL FEATURES OF THE TURBULENT FLOW OF A VISCOELASTIC FLUID FOR REDUCED DRAG

L. Thais
Université de Lille Nord de France, USTL
F59000 Lille, France
Laboratoire de Mécanique de Lille
CNRS, UMR 8107
F59655 Villeneuve d'Ascq, France
laurent.thais@polytech-lille.fr

T. B. Gatski
Institut Pprime
CNRS–Université de Poitiers–ENSMA
F86036 Poitiers cedex, France
Center for Coastal Physical Oceanography
Old Dominion University
Norfolk, Virginia 23529 USA
thomas.gatski@univ-poitiers.fr

G. Mompean
Université de Lille Nord de France, USTL
F59000 Lille, France
Laboratoire de Mécanique de Lille
CNRS, UMR 8107
F59655 Villeneuve d'Ascq, France
Gilmar.Mompean@polytech-lille.fr

ABSTRACT

It is well-known that the addition of minute amounts of long polymer chains to organic solvents, or water, can lead to significant turbulent drag reduction (DR). In the present study, direct numerical simulations (DNS) of turbulent channel flow of a viscoelastic fluid, at friction Reynolds numbers ranging from 180 to 1000, are further analyzed. The analysis is focused on the turbulent stress and viscoelastic extra-stress (conformation tensor) fields in order to contrast the dynamics of the viscoelastic and Newtonian fluids and to quantify the effects of enhanced elasticity on the viscoelastic extra-stress fields. The simulation results coupled with the analyzes just mentioned can be useful in further assessing the underlying mechanisms responsible for the occurrence of drag reduction.

INTRODUCTION

The numerical simulation of the drag reduction phenomenon by polymer additives has been actively pursued for over a decade. The first such direct numerical simulation with a viscoelastic fluid were performed by Sureshkumar *et al.* (1997). The simulation was of a fully developed channel flow at a $Re_{\tau0}$ of 125 using the FENE-P model (Finitely Extensible Non-linear Elastic in the Peterlin approximation), appropriate for dilute polymer solutions. Additional studies followed using other fluids and flow conditions (e.g. Dimitropoulos *et al.*, 1998; Dubief *et al.*, 2004; Housiadas & Beris, 2003, 2006). Dimitropoulos *et al.* (2001) performed a detailed analysis of the budget of turbulent kinetic energy and streamwise enstrophy for the FENE-P solution. They showed that the inhibition of vortex stretching, which is a consequence of the high extensional viscosity of the polymer solution, is a possible mechanism responsible for drag reduction. Using the Oldroyd-B model, Min *et al.* (2003*b*) (see also Min *et al.*, 2003*a*) predicted the onset of drag reduction at friction Weissenberg numbers in agreement with those from experiments. In contrast, they proposed an elastic theory in which the polymer stores turbulent energy near the wall and releases it further away when the elastic time scale is sufficiently long.

Just as in turbulent Newtonian flows, such direct numerical simulations have limited engineering usefulness. Constraints imposed by the small scale resolution required at high Reynolds numbers are augmented by constraints imposed by increasing Weissenberg numbers (fluid relaxation time scale to mean flow time scale) and maximum polymer chain elongation lengths *L*. This has led to the development of Reynolds-averaged (RANS) closure modeling. Lowest-order models have been proposed by Li *et al.* (2006) (an algebraic, zero-equation, eddy viscosity model). Cruz *et al.* (2004) formulated a two-equation $k - \varepsilon$ closure with modified shear-thinning fluid properties. Intermediate to the RANS modeling and DNS, Thais *et al.* (2010) performed a novel large eddy simulation of viscoelastic turbulent channel flow. They utilized a temporal filtering approach that allowed them to achieve maximum chain extensibility for the FENE-P model of 100 and a zero-shear friction Weissenberg number up to 116, but at a relatively modest zero-shear friction Reynolds number of 180. The drag reduction results obtained from this (T)LES agreed with DNS results at the same conditions. The development of such low-order engineering models requires

DNS at relatively high Reynolds numbers, and it is the results of these simulations which is the focus of the present contribution.

FORMULATION

The incompressible flow field under consideration is a fully developed turbulent channel flow of a FENE-P viscoelastic fluid. The channel streamwise direction is $x_1 = x$, the wall-normal direction is $x_2 = y$, and the spanwise direction $x_3 = z$. The instantaneous velocity field is $(u, v, w) = (u_1, u_2, u_3)$, and the variables are scaled with the bulk velocity $\langle U_b \rangle$ and the channel half-height h. The channel is also assumed of infinite extent in the spanwise direction.

Momentum Equation

The dimensionless momentum conservation equation is given by

$$\frac{\partial u_i}{\partial t} + u_j \frac{\partial u_i}{\partial x_j} = -\frac{\partial p}{\partial x_i} + \frac{\beta_0}{Re_b} \frac{\partial^2 u_i}{\partial x_j^2} + \frac{(1-\beta_0)}{Re_b} \frac{\partial \tau_{ij}}{\partial x_j} + e_i \delta_{i1},$$
(1)

where the bulk Reynolds number is $Re_b = \rho \langle U_b \rangle h / \eta_0$, $\beta_0 = \eta_s / \eta_0$, and $\eta_0 = \eta_s + \eta_{p0}$ is the total zero-shear rate viscosity (η_{p0} is the polymeric zero-shear rate viscosity). A uniform polymer concentration is assumed and is characterized by the viscosity ratio β_0 (the limit $\beta_0 = 1$ is a Newtonian fluid). The solvent to total viscosity ratio was here fixed to $\beta_0 = 0.9$. The quantity $e_i \delta_{i1}$ is the driving pressure gradient in the streamwise channel direction x_1.

Conformation Tensor

The extra-stress τ_{ij} in Eq. (1) is related to the conformation tensor components c_{ij}, which represent the ensemble average squared norm of the end-to-end vector of polymer molecules. The extra-stress and conformation tensor relationship for the FENE-P fluid is given by

$$\tau_{ij} = \frac{f(\{\mathbf{c}\}) c_{ij} - \delta_{ij}}{We_b},$$
(2)

where $f(\{\mathbf{c}\})$ is the Peterlin approximation,

$$f(\{\mathbf{c}\}) = \frac{L^2 - 3}{L^2 - \{\mathbf{c}\}},$$
(3)

with L the maximum chain extensibility, $\{\mathbf{c}\} = c_{ii}$ the trace of the conformation tensor, and $We_b = \lambda \langle U_b \rangle / h$ the bulk Weissenberg number. The governing equation for the conformation tensor is

$$\frac{\partial c_{ij}}{\partial t} + u_k \frac{\partial c_{ij}}{\partial x_k} - \frac{\partial u_i}{\partial x_k} c_{kj} - \frac{\partial u_j}{\partial x_k} c_{ki} = \frac{\delta_{ij} - f(\{\mathbf{c}\}) c_{ij}}{We_b}$$
$$+ \left(\frac{1}{Pr_c Re_b} \right) \frac{\partial^2 c_{ij}}{\partial x_k^2} \quad (4)$$

where $Pr_c = \eta_0 / \rho \kappa_c$ is an extra-stress Prandtl number defined as the ratio of the total kinematic zero-shear rate viscosity (η_0 / ρ) to a numerical stress diffusivity κ_c. Viscoelastic simulations utilizing Eq. (4) require a numerical stabilization term (Sureshkumar & Beris, 1995) in order to effectively compute flows over a range of Weissenberg numbers. For the simulations reported here, the stress Prandtl number was chosen to yield a diffusivity of $1/(Pr_c Re_b) = 3.5 \times 10^{-4}$ in Eq. (4) at the highest Reynolds number considered (see Thais *et al.*, 2011, for details of the simulations and numerical scheme used).

RESULTS

A wide range of fully developed channel flow numerical simulations have been performed contrasting the behavior of Newtonian and viscoelastic (FENE-P) fluids in a channel of length $L_x = 8\pi$ allowing a high drag reduction regime. The zero-shear frictional Reynolds numbers, $Re_{\tau 0} (= u_{\tau 0} h / \eta_0)$ in the simulations have ranged from 180 to 1000, with a common friction Weissenberg number, $We_{\tau 0} (= \rho \lambda u_{\tau 0}^2 h / \eta_0)$ of 116 and a maximum chain extension length $L = 100$. The DR for the various Reynolds number cases have been: $Re_{\tau 0} = 180$, $DR = 64\%$; $Re_{\tau 0} = 395$, $DR = 62\%$; $Re_{\tau 0} = 590$, $DR = 61\%$; $Re_{\tau 0} = 1000$, $DR = 58\%$. The statistical correlations to be presented have been averaged in time as well as in the streamwise and spanwise homogeneous directions, with the components of the Reynolds stress tensor defined by $T_{ij} = \overline{u_i' u_j'}$. Both the extra-stress tensor, τ_{ij}, and conformation tensor, c_{ij} are partitioned into a mean, $\overline{\tau}_{ij}$ and $\overline{c}_{ij}$, and fluctuating parts, τ_{ij}' and c_{ij}'. Although the focus here will be on the turbulent second-moments and conformation (extra-stress) tensor, it is worthwhile at the outset to see the influence of increasing $Re_{\tau 0}$ on the mean velocity of the FENE-P fluid flow. Figure 1 shows the variation of the mean velocity across the channel half-width. For the lower $Re_{\tau 0}$ values of 180, 395, and 590, there is minimal, if any, sign of an initial log-law region. Only at $Re_{\tau 0} = 1000$ does a log-law region begin to appear. Such behavior suggests a significant extension of the sublayer buffer layer regions into the channel. While it is clear the FENE-P fluid has had a significant effect on the mean velocity profile, this should not be construed as an overall reduction of the turbulence itself. The dynamic interactions between the viscoelastic fluid dynamics and the turbulent flow dynamics results in this mean velocity alteration relative to the Newtonian fluid. In the remainder of this paper, the focus will be on the respective turbulent flow and viscoelastic fluid statistical features.

Turbulent Flow Dynamics

The turbulence dynamics are significantly affected by the inclusion of viscoelastic fluid effects. A measure of this is provided by examining the turbulent kinetic energy, $k_t (= T_{ii}/2)$, in the Newtonian and viscoelastic fluid flows. Figure 2 shows this distribution across the channel half-width (in wall-units) and compares the influence of increasing $Re_{\tau 0}$ between the Newtonian and FENE-P fluids. As the figure shows, there is a significant increase (almost double) in peak amplitude of the kinetic energy for the FENE-P fluid. Additionally, relative to the Newtonian case, there is a shift of peak amplitude location away from the channel wall for the viscoelastic fluid;
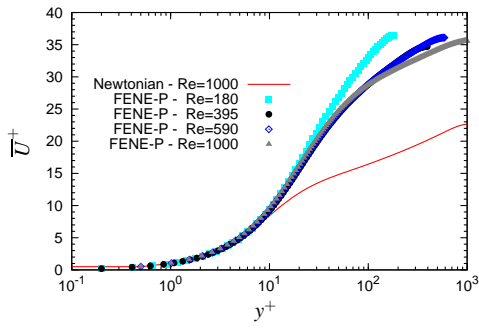
Figure 1. Variation of mean velocity profile with friction Reynolds number: FENE-P fluid, $L = 100$, $We_{\tau 0} = 116$.
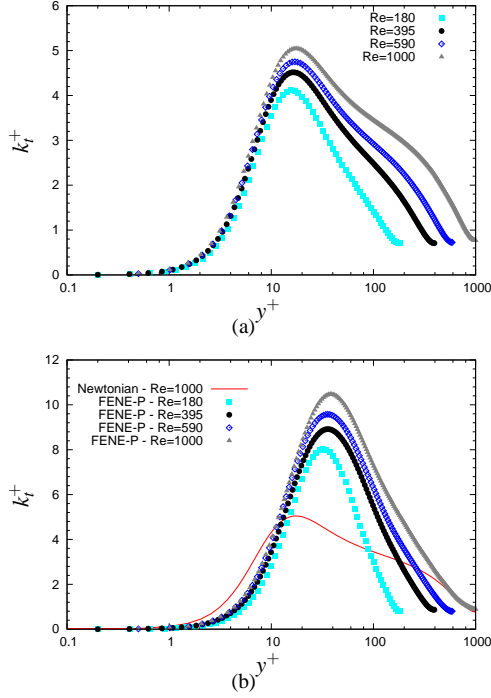
Figure 2. Turbulent kinetic energy: (a) Newtonian fluid; (b) FENE-P fluid, $L = 100$, $We_{\tau 0} = 116$.

although, the peak location tends to vary little with increasing $Re_{\tau 0}$. Additional insight can be gained into the dynamics by examining the distribution of the component normal stresses.

Figures 3 – 5 show the Reynolds normal stress components. Overall, for each Reynolds stress component, there is an increase in magnitude with increasing $Re_{\tau 0}$ for both the Newtonian and viscoelastic fluids. The Newtonian behavior is in line with independent simulations by Hoyas & Jiménez (2006) up to $Re_{\tau 0} = 2000$. However, for the streamwise component T_{xx}^+, the values for the viscoelastic fluid are almost double those of the Newtonian values (see Fig. 3); whereas, for the wall-normal and spanwise components there is a decrease in the values relative to the Newtonian fluid (see Figs. 4 and 5). This increase in streamwise Reynolds normal stress component is consistent with the increase found in the turbulent kinetic energy distribution.

For the wall-normal and spanwise Reynolds stress components, there is a decrease of approximately 50% in the
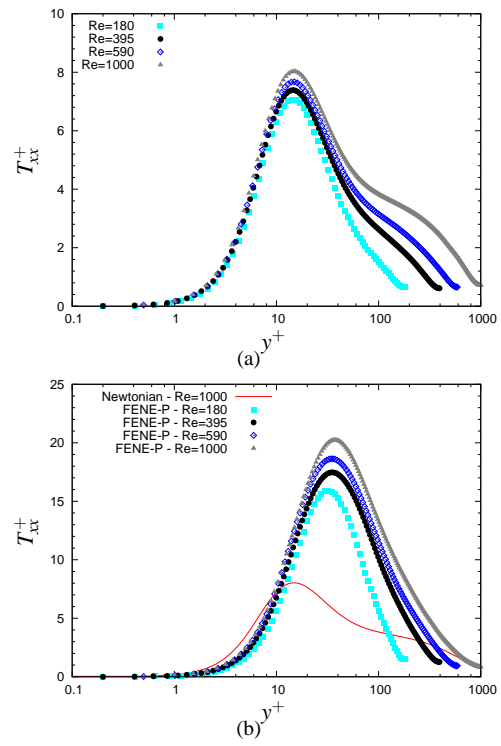
Figure 3. Streamwise Reynolds normal stress component: (a) Newtonian fluid; (b) FENE-P fluid, $L = 100$, $We_{\tau 0} = 116$.

maximum value at $Re_{\tau 0} = 1000$ from the Newtonian to the FENE-P fluid (see Figs. 4(b) and 5(b)). In contrast, there is a relative increase, at the same $Re_{\tau 0} = 1000$ value for the streamwise component between the Newtonian and FENE-P fluids as shown in Fig. 3(b). These results suggest that the turbulent stress anisotropy is influenced by the inclusion of viscoelastic effects. In addition, the location of the peak Reynolds normal stress values are shifted away from the channel wall for the FENE-P fluid for each normal stress component; however, this shift is more enhanced, and dependent on Reynolds number, for the wall-normal and spanwise components than the streamwise normal stress component.

For the Reynolds shear stress component T_{xy}^+, a similar reduction to that observed for the T_{yy}^+ and T_{zz}^+ normal stress components is shown in Fig. 6. The reduction in peak magnitude for the $Re_{\tau 0} = 1000$ case is about 33% as compared to the almost 50% for the normal stresses T_{yy}^+ and T_{zz}^+. Figure 6 also shows a relatively minor shift away from the channel wall in the location of the peak shear stress magnitude with increasing $Re_{\tau 0}$.

The discussion of the turbulence dynamics can be augmented by examining the Reynolds stress anisotropy invariants and an invariant map of the second- and third-invariants. The Reynolds stress anisotropy is given by $b_{ij} = T_{ij}/T_{ii} - \delta_{ij}/3$ with the second, II_b, and third, III_b, invariants defined by $II_b = -b_{ij}b_{ji}/2$ and $III_b = b_{ij}b_{jk}b_{ki}/3$. The Reynolds stress anisotropy invariant maps are shown in Fig. 7 at $Re_{\tau 0} = 590$. Relative to the behavior of the Newtonian fluid, the distribution across the channel for the FENE-P fluid is quite different. The Newtonian distribution near the wall lies along the two-component boundary where the T_{xx} and T_{zz} components dominate with a bias towards the axisymmetric boundary. In

3
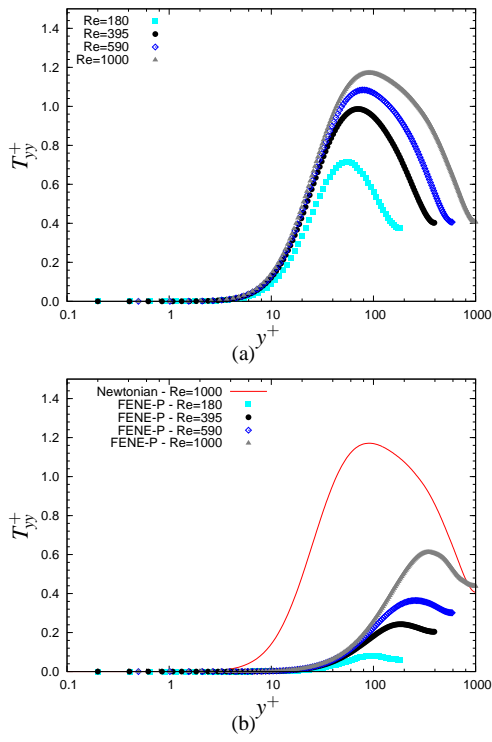
Figure 4. Wall-normal Reynolds normal stress component: (a) Newtonian fluid; (b) FENE-P fluid, $L = 100$, $We_{\tau 0} = 116$.
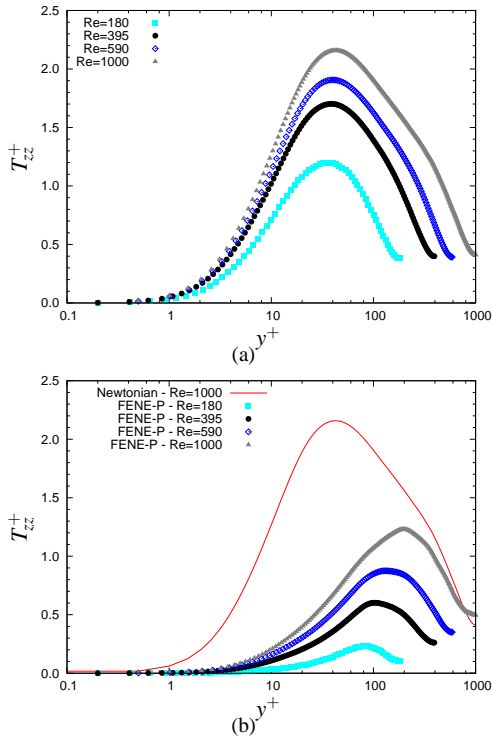
Figure 5. Spanwise Reynolds normal stress component: (a) Newtonian fluid; (b) FENE-P fluid, $L = 100$, $We_{\tau 0} = 116$.
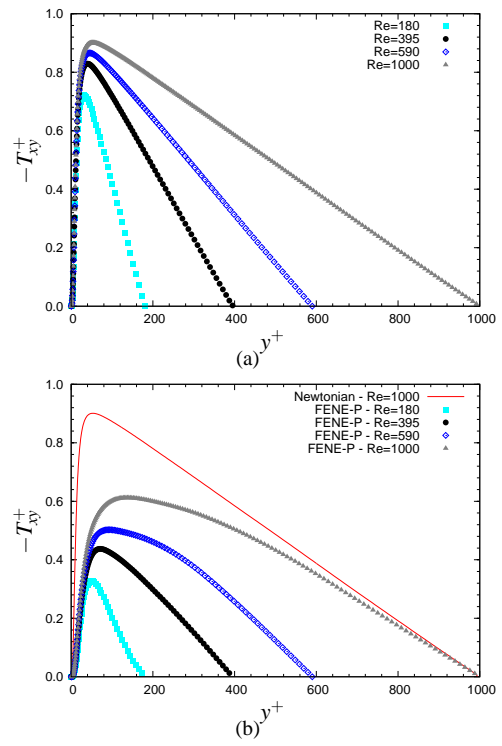
Figure 6. Reynolds shear stress component: (a) Newtonian fluid; (b) FENE-P fluid, $L = 100$, $We_{\tau 0} = 116$.

contrast, for the FENE-P fluid the bias is toward the one-component limit implying an enhanced retardation of the T_{zz} component. The migration from the two-component boundary toward the axisymmetric boundary occurs at $y^+ = 8$ for the Newtonian case, but for the FENE-P fluid the invariants lie along the axisymmetric boundary from $y^+ = 16$. In addition, the anisotropy distribution for the FENE-P fluid approaches the one-component limit showing a significant suppression of the wall-normal and spanwise normal stress components relative to the streamiwse component. Since the characteristic velocity scale appropriate to an estimate for the turbulent eddy viscosity is the square root of the wall-normal component T_{yy}, this result suggests a diminished influence of the turbulence on the mean flow (see Fig. 1). Near the channel centerline, the invariant distributions approach the isotropic limit for Newtonian flow; whereas, for the FENE-P fluid the streamwise stress component is still sufficiently dominant over the other stress components for the invariant map at the centerline to terminate along the axisymmetric boundary.

Viscoelastic Fluid Dynamics

From Eqs. (2) and (4), the distribution of the conformation tensor governs the influence of the viscoelastic fluid on the flow dynamics through the extra-stress tensor. In particular, the normal components of the conformation tensor are the dominant contributors to this polymeric influence. As Fig. 8 shows, the streamwise normal component of the c_{ij} dominates (by more than an order of magnitude) over a large portion of the channel half-width relative to the other normal components. Even with the dominance in magnitude of $\overline{c}_{xx}$, Benzi (2010) has recently shown that the wall-normal component
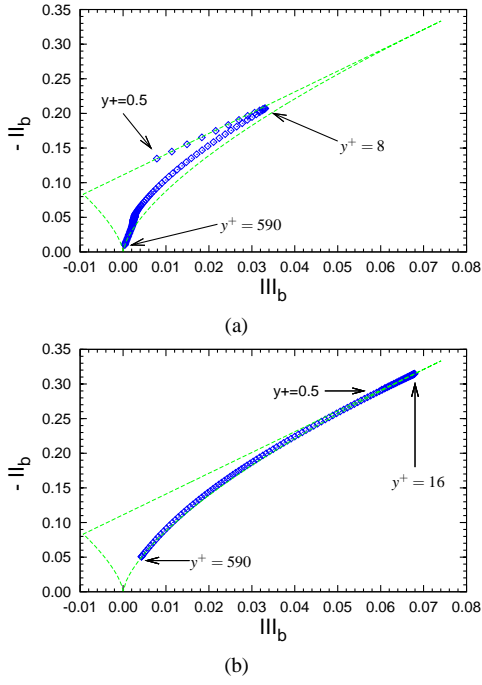
Figure 7. Reynolds stress anisotropy invariant map at $Re_{\tau 0} = 590$: (a) Newtonian fluid; (b) FENE-P fluid, $L = 100$, $We_{\tau 0} = 116$.

Figure 8. Normal components of conformation tensor for FENE-P fluid, $Re_{\tau 0} = 590$, $L = 100$, $We_{\tau 0} = 116$: (a) Streamwise component; (b) Wall-normal, ○, and spanwise, ×, components.

$\overline{c}_{yy}$ is the dominant contributor to an effective polymeric viscosity that strongly influences the turbulent dynamics in the inner layer. While this effective viscosity is not a turbulent eddy viscosity, the dependence on the wall-normal component is consistent with near-wall turbulent modeling concepts that recognize that the wall-normal Reynolds stress component is the relevant velocity scale in the inner layer near the wall. Figure 8(b) shows there is only a weak linear variation of both the $\overline{c}_{yy}$ and $\overline{c}_{zz}$ components, and this only occurs in a relatively narrow region of the inner layer ($10 < y^+ < 20$ for the $\overline{c}_{yy}$ component and $25 < y^+ < 35$ for the $\overline{c}_{zz}$ component). This is in contrast with the theoretical proposal of Benzi (2010) who estimated a linear behavior over a larger portion of the near-wall region, and also predicted a y^{-1} behavior for the $\overline{c}_{xx}$ component, keeping in mind that his theory utilizes a simplified fluid model which mimics partially viscoelastic effects.

The extra-stress anisotropy $e_{ij} = \overline{\tau}_{ij}/\overline{\tau}_{ii} - \delta_{ij}/3$ can also be analyzed through a corresponding anisotropy invariant map shown in Fig. 9. The extra-stress induces a strong elongation effect in the streamwise direction which is consistent with the large values of the corresponding conformation tensor component. Since the figure is a phase-plane of invariants, it provides information on the principal rates of strain of the extra-stress tensor and also shows that in the principal directions normal to the streamwise direction, the corresponding eigenvalues are approximately equal and of the same sign ($e_{ii} = 0$). Although Fig. 8(b) for the wall-normal and spanwise components of the conformation tensor (extra-stress tensor) show unequal distributions across the channel, this is not inconsistent with the eigenvalue behavior, since the eigenvalues are the principal stretches along the principal directions. These
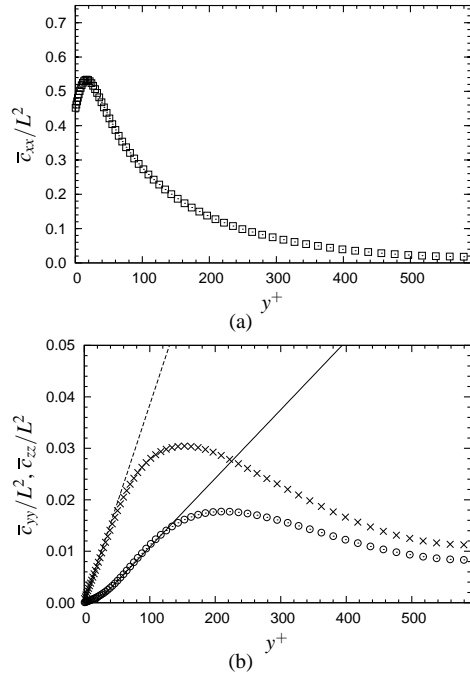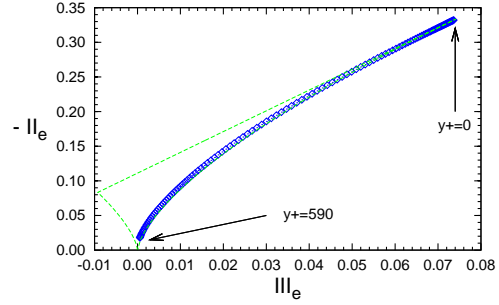
Figure 9. FENE-P extra-stress anisotropy invariant map: $Re_{\tau 0} = 590$, $L = 100$, $We_{\tau 0} = 116$.

principal axes are related to the y and z axes through a simple rotation.

The elastic energy is given by $k_e = (1 - \beta_0)\overline{\tau}_{ii}/(2Re_b)$ and is extracted directly from the conformation tensor using Eq. (2). It is governed by a dynamic balance between production and dissipation as

$$\frac{Dk_e}{Dt} = P_{em} + P_{et} - \varepsilon_e , \qquad (5)$$

where $P_{em} = (1 - \beta_0)/Re_b \, \overline{\tau}_{xy} \, \partial \overline{U}/\partial y$ is the production of elastic energy by the mean flow, $P_{et} = (1 - \beta_0)/Re_b \, \overline{\tau'_{ij} \partial u'_i/\partial x_j}$ is the production of elastic energy by the fluctuating extra-stress, and $\varepsilon_e = k_e/We_b$ is the elastic energy dissipation rate. The form of the elastic energy dissipation rate

5
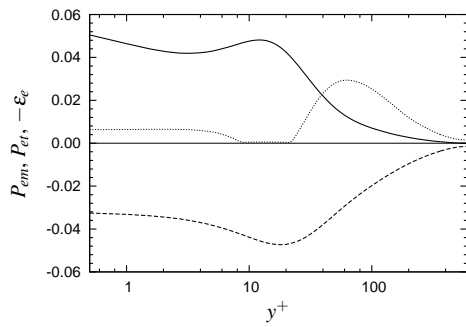
Figure 10. Elastic energy budget for FENE-P fluid, $L = 100$, $We_{\tau 0} = 116$: ——, P_{em}, production of elastic energy by the mean flow; ······, P_{et}, production of elastic energy by turbulence; dashed line − − −, ε_e, dissipation of elastic energy.

is analogous to an inertial estimate for the turbulent kinetic energy dissipation rate given by k_t/T_t, where T_t is a turbulent time scale. Figure 10 shows the balance of terms for the elastic energy across the channel half-width at $Re_{\tau 0} = 590$. Similar to the turbulent kinetic energy distribution in Fig. 2, the elastic energy (which is proportionnal to the long-dashed line in Fig 10) has relatively slow growth with distance from the wall, and then increases more rapidly in the buffer layer region where a peak value is reached at $y^+ \approx 20$. From this peak value there is a continuous decrease throughout the channel toward the centerline.

While the qualitative balance between the mean production and elastic energy dissipation rate is apparent in the figure, the production of elastic energy by the fluctuating extra-stress displays a unique behavior in the range $10 < y^+ < 30$ where its contribution to the dynamic balance effectively vanishes.

CONCLUDING REMARKS

Finally, it would be remiss not to make some comments concerning two prominent long-standing explanations for the mechanism of polymer drag reduction proposed by Lumley (1969) and Tabor & De Gennes (1986). Lumley's 1969 explanation assumes the affect of polymer stretching in a turbulent flow produces an increase in the effective viscosity in a region outside of the viscous sublayer and in the buffer layer. Tabor and De Gennes's 1986 explanation assumes that the elastic energy stored by the polymer becomes comparable to the kinetic energy in the buffer layer. The corresponding viscoelastic length scale is larger than the Kolmogorov scale which inhibits the usual energy cascade and thickens the buffer layer. It is not a simple matter to assess these two explanations since the results here show that the turbulent flow dynamics are coupled with the FENE-P fluid dynamics (elastic effects) in a manner that is not yet known with certainty. The simulation results shown display an increase in turbulent kinetic energy and elastic energy in the critical buffer layer region; however, the dynamic balance causing this needs further investigation. Even with this information, improved estimates are needed for the effective viscosity which have a direct impact on the influence of the extra-stress on the mean velocity field.

REFERENCES

Benzi, R. 2010 A short review on drag reduction by polymers in wall bounded turbulence. *Physica D* **239**, 1338–1345.

Cruz, D. O. A., Pinho, F. T. & Resende, P. R. 2004 Modeling the new stress for improved drag reduction predictions of viscoelastic pipe flow. *J. Non-Newtonian Fluid Mech.* **121**, 127.-141.

Dimitropoulos, C. D., Sureshkumar, R. & Beris, A. N. 1998 Direct numerical simulation of viscoelastic turbulent channel flow exhibiting drag reduction: effect of the variation of rheological parameters. *J. Non-Newtonian Fluid Mech.* **79**, 433–468.

Dimitropoulos, C. D., Sureshkumar, R., Beris, A. N. & Handler, R. A. 2001 Budgets of Reynolds stress, kinetic energy and streamwise enstrophy in viscoelastic turbulent channel flow. *Phys. Fluids* **13(4)**, 1016–1024.

Dubief, Y., White, C. M., Terrapon, V. E., Shakfeh, E. S. G., Moin, P. & Lele, S. K. 2004 On the coherent drag-reducing and turbulence-enhancing behaviour of polymers in wall flows. *J. Fluid Mech.* **514**, 271–280.

Housiadas, K. D. & Beris, A. N. 2003 Polymer-induced drag reduction: Effects of the variations in elasticity and inertia in turbulent viscoelastic channel flow. *Phys. Fluids.* **15**, 2369–2384.

Housiadas, K. D. & Beris, A. N. 2006 Extensional behavior influence on viscoelastic turbulent channel flow. *J. Non-Newtonian Fluid Mech.* **140**, 41–56.

Hoyas, S. & Jiménez, J. 2006 Scaling of velocity fluctuations in turbulent channels up to $Re_\tau = 2000$. *Phys. Fluids* **18**, 011702.

Li, C.-F., Gupta, V. K., Sureshkumar, R. & Khomami, B. 2006 Turbulent channel flow of dilute polymeric solutions: drag reduction scaling and an eddy viscosity model. *J. Non-Newtonian Fluid Mech.* **139**, 177–189.

Lumley, J. L. 1969 Drag reduction by additives. In *Annu. Rev. Fluid Mech.*, pp. 367–384. New York: Annual Reviews.

Min, T., Yoo, J. Y. & Choi, H. 2003a Maximum drag reduction in a turbulent channel flow by polymer additives. *J. Fluid Mech.* **492**, 91–100.

Min, T., Yoo, J. Y., Choi, H. & Joseph, D. D. 2003b Drag reduction by polymer additives in a turbulent channel flow. *J. Fluid Mech.* **486**, 213–238.

Sureshkumar, R. & Beris, A. N. 1995 Effect of artificial stress diffusivity on the stability of numerical calculations and the dynamics of time-dependent viscoelastic flows. *J. Non-Newtonian Fluid Mech.* **60**, 53–80.

Sureshkumar, R., Beris, A. N. & Handler, R. A. 1997 Direct numerical simulation of the turbulent channel flow of a polymer solution. *Phys. Fluids* **9**, 743–755.

Tabor, M. & De Gennes, P. G. 1986 A cascade theory of drag reduction. *Europhys. Lett.* **2**, 519–522.

Thais, L., Tejada-Martinez, A., Gatski, T. B. & Mompean, G. 2010 Temporal large eddy simulations of turbulent viscoelastic drag reduction flows. *Phys. Fluids* **22**, CID 013103.

Thais, L., Tejada-Martinez, A., Gatski, T. B. & Mompean, G. 2011 A massively parallel hybrid scheme for direct numerical simulation of turbulent viscoelastic channel flow. *Computers and Fluids* **43**, 134–142.